Journal of Simulation and Analysis of Novel Technologies in Mechanical Engineering
17 (3) (2025) 0039~0051
DOI 10.71939/jsme.2025.1214765

Numerical simulation of heat transfer in liver tumor therapy using magnetic nanoparticles under alternating magnetic fields

Hamoon Pourmirzaagha*, Parimah Salimi

Department of Mechanical and Aerospace Engineering, Ram.C., Islamic Azad University, Ramsar, Iran

*Hamoon.pourmirzaagha@iau.ac.ir

(Manuscript Received --- 13 Aug. 2025; Revised --- 25 Nov. 2025; Accepted --- 01 Dec. 2025)

Abstract

Cancer is a major global health challenge that necessitates targeted therapeutic approaches with minimal damage to healthy tissues. Hyperthermia, by locally elevating the temperature of cancerous tissue to approximately 42–45°C, enhances tumor cell sensitivity to radiotherapy and chemotherapy, ultimately inducing selective cell death. In this study, magnetic hyperthermia using iron oxide magnetic nanoparticles (MNPs) combined with an alternating magnetic field (AMF) is employed as a non-invasive and effective method for liver cancer treatment. Heat transfer modeling within liver tissue containing MNPs was conducted using the COMSOL Multiphysics environment. Key parameters such as nanoparticle type, particle diameter, magnetic field frequency, and applied power intensity were investigated. The results demonstrated that increasing the magnetic field intensity and frequency leads to a higher heating rate and greater thermal damage to tumor tissue. These findings suggest that optimal utilization of magnetic nanoparticles could serve as an effective strategy for non-invasive treatment of deep-seated tumors like liver cancer.

Keywords: Magnetic nanoparticles, Liver cancer, Magnetic hyperthermia, Heat transfer simulation, Alternating magnetic field

1- Introduction

Cancer is one of the most critical public health challenges worldwide, responsible for millions of deaths annually and imposing substantial economic, psychological, and social burdens on societies. This complex disease arises when normal cellular genetic regulation is disrupted, leading cells to deviate from controlled proliferation and programmed cell death (apoptosis). Under physiological conditions, cell division is tightly regulated, allowing new cells to replace senescent or damaged ones. However, any disruption in this process can result in the formation of abnormal cell masses, which may manifest as benign or malignant tumors. Malignant tumors exhibit aggressive growth, invading adjacent tissues and potentially disseminating to distant organs via the bloodstream or lymphatic system—a process known as metastasis—which considerably complicates therapeutic interventions.

Conventional cancer treatments, including surgery, chemotherapy, and radiotherapy, though often effective, are associated with collateral damage to surrounding healthy tissues, the development of drug resistance, tumor recurrence, and reduced patient

quality of life. Consequently, recent years have seen increasing interest in novel, targeted, and minimally invasive therapeutic modalities with fewer side effects. Among these, hyperthermia—controlled elevation of temperature within the tumor region—has emerged as a promising approach to selectively induce cancer cell death.

Numerous studies have demonstrated that hyperthermia in the range of 42–46°C disrupts critical cellular functions such as membrane integrity, enzymatic activity, and protein structures, leading to cancer cell death via necrosis or apoptosis [1–4]. Furthermore, hyperthermia enhances the intracellular uptake of chemotherapeutic agents and sensitizes tumors to radiation therapy, all while exhibiting significantly fewer adverse effects compared to traditional treatments. Various techniques have been proposed to deliver therapeutic heat to target tissues. Radiofrequency (RF) ablation, one of the most commonly used methods, generates heat through high-frequency alternating currents passing through tissues [5–8]. While minimally invasive and yielding satisfactory outcomes in many cases, RF ablation is limited by shallow penetration depth, dependency on direct electrode-tissue contact, and potential damage to adjacent healthy tissues. Microwave ablation offers an alternative by exciting water molecules within tissues to produce more uniform heating, making it particularly effective for solid tumors such as hepatic, pulmonary, and breast cancers [9, 10]. This technique provides high efficacy, can treat tumors near large vessels, and allows simultaneous ablation of multiple sites. However, similar absorption by both malignant and healthy tissues may cause unintended damage and limit treatment precision [11]. High-Intensity Focused Ultrasound (HIFU) is a non-invasive, highly precise technique that concentrates ultrasonic waves at a focal point deep within the body, raising temperatures locally without harming superficial layers, thereby ablating cancerous cells [12, 13]. Despite its advantages, challenges such as energy dispersion, decreased efficacy in highly perfused areas, and difficulties in precisely controlling thermal distribution remain.

Laser-induced thermal therapy (LITT) delivers localized heat by guiding thin optical fibers directly into tumors to induce thermal ablation [14, 15]. While offering high spatial accuracy, this invasive method risks injury to vital structures and uneven heat distribution.

In the last decade, nanotechnology-based approaches have gained attention, particularly magnetic nanoparticles (MNPs) activated by alternating magnetic fields (AMFs) for localized hyperthermia [16–23]. In this strategy, MNPs are either targeted or directly injected into tumors, where exposure to AMFs generates heat via nanoparticle rotation or internal friction. This technique boasts deep tissue penetration, precise temperature control, and minimal damage to surrounding healthy tissues, positioning it as a promising future modality—especially for hepatic tumors.

The liver's complex anatomy, extensive vasculature, and central metabolic role render tumor treatment particularly challenging. Non-uniform heat distribution, thermal washout due to high perfusion, and collateral damage to healthy tissue constitute major hurdles in conventional methods. Magnetic nanoparticle-mediated hyperthermia enables selective, safe, and sustained

thermal ablation, overcoming many of these challenges.

This study aims to develop an advanced and detailed computational model of heat transfer in liver tissue embedded with magnetic nanoparticles under alternating magnetic stimulation. Unlike most previous numerical studies that considered simplified or homogeneous tissue domains, the present work incorporates realistic hepatic geometry and physiological thermal properties to more accurately predict temperature distribution and tissue response. By employing COMSOL Multiphysics as a robust multiphysics platform, the model investigates the combined effects of magnetic field intensity, frequency, nanoparticle type, and tissue-specific characteristics on heat generation and thermal injury. This approach represents a meaningful advancement beyond conventional hyperthermia simulations, bridging the gap between theoretical modeling and physiologically realistic conditions, and providing new understanding relevant to clinical applications in liver cancer therapy.

2- Problem definition

Figure 1, a schematic illustration of the Magnetic Fluid Hyperthermia (MFH) process applied to a liver tumor, demonstrates the targeted accumulation of magnetic nanoparticles and the resulting localized thermal effect.

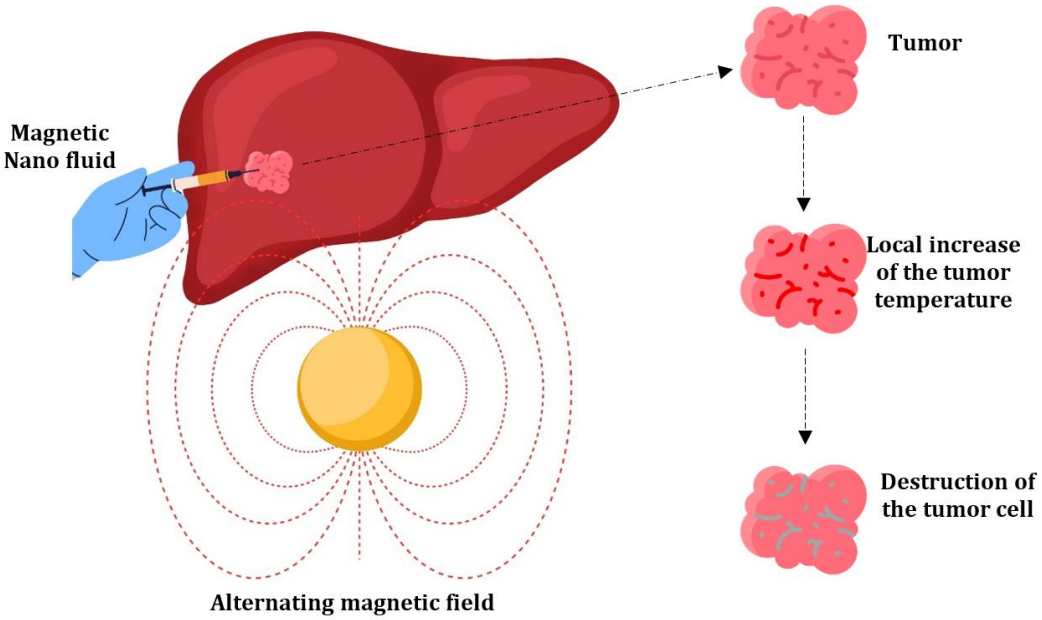

Fig. 1 A schematic view of the MFH process of a liver tumor

2-1- Geometry

For modeling the hyperthermia process utilizing magnetic nanoparticles, a three-dimensional geometry was constructed to accurately represent the physical structure of the liver and the tumor region, as illustrated in Fig. 2. To enhance the numerical solution accuracy, a non-uniform meshing strategy was employed, balancing computational efficiency with precision. Fig. 3 depicts the meshing configuration, highlighting a higher mesh density concentrated around the nanoparticle injection site to capture localized thermal effects with greater detail.

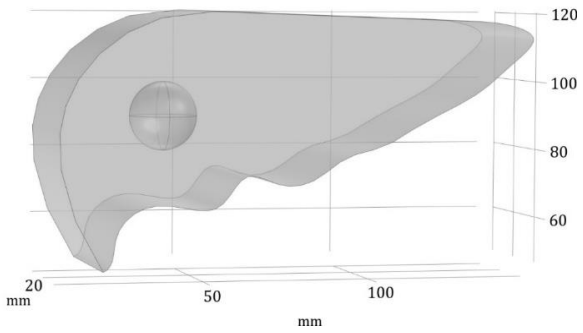

Fig. 2 Three-dimensional representation of the modeled geometry, including the liver tissue and the tumor region

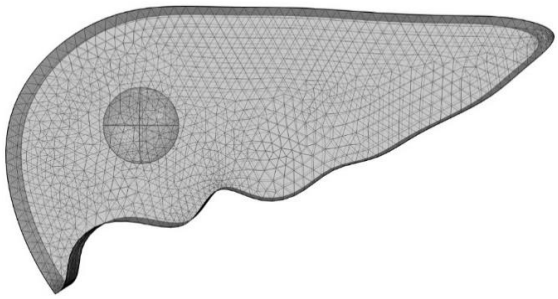

Fig. 3 Mesh representation of the model

2-2- Governing equations

To obtain the temperature distribution during hyperthermia treatment, it is essential to solve the energy equation within the target tissue domain, applying the appropriate boundary conditions. The Pennes bioheat transfer equation for both tumor and healthy tissue can be expressed as follows [24]:

$$\rho_1 c_1 \frac{\partial T}{\partial t} = k_t \nabla^2 T + (\rho c)_b w_b (T_a - T) ... + Q_{met} + P \quad (1)$$

$$\rho_2 c_2 \frac{\partial T}{\partial t} = k_t \nabla^2 T + (\rho c)_b w_b (T_a - T) ... + Q_{met} + P \quad (2)$$

Eq. (1) is applied to the tumor region, while Eq. (2) is used for the healthy tissue. In these equations, the density and specific heat capacity of the tumor (subscript 1), the tissue (subscript 2), and the nanoparticles (subscript M with volume fraction φ) are assumed as follows:

$$\rho_1 = \varphi \rho_M + (1-\varphi)\rho_2 \quad (3)$$

$$c_{P1} = \varphi c_{PM} + (1-\varphi) c_{P2} \quad (4)$$

The heat generation by the magnetic nanoparticle is assumed as follows [25]:

$$P = \mu_0 \pi \chi_0 f H^2 \frac{2\pi f \tau}{1 + (2\pi f \tau)^2} \quad (5)$$

Here, μ_0 denotes the permeability of free space, χ_0 represents the magnetic susceptibility and H refers to the strength of the alternating magnetic field. Since both Brownian and Néel relaxations contribute to the effective relaxation time τ, the heat generation expression is given as follows [25]:

$$\tau = \frac{\tau_B \tau_N}{\tau_B + \tau_N} \quad (6)$$

Here, τ_N and τ_B denote the Néel and Brownian relaxation times, respectively. In the Brownian relaxation mechanism, the magnetic moment is coupled to the crystal axis and causes the entire nanoparticle to physically rotate when aligning with the external magnetic field. In contrast, the Néel relaxation involves internal rotation of the magnetic moment within the crystal structure without physical motion of the particle. To achieve higher heat generation rates, dominance of the Néel relaxation mechanism is generally undesirable. The Brownian relaxation time is defined by the following relation [25]:

$$\tau_B = \frac{3\eta V_H}{k_b T} \quad (7)$$

In this equation, η represents the viscosity of the carrier fluid (in this case, water), and the hydrodynamic volume of the nanoparticle is defined as $V_H = \pi(D+2)^3/6$, where D is the diameter of the

nanoparticle, k_b is the Boltzmann constant, and T denotes the absolute temperature. The Néel relaxation time is expressed as follows:

$$\tau_N = \frac{\sqrt{\pi}}{2}\tau_0 \frac{\exp(\Gamma)}{\sqrt{\Gamma}} \quad (8)$$

$$\Gamma = \frac{kV_M}{k_b T} \quad (9)$$

In this equation, K denotes the magnetic anisotropy constant, V_M is the volume of the nanoparticle, T represents the absolute temperature, and $\tau_0 = 10^{-9}$ is the characteristic relaxation time [25].

Moreover, the equilibrium magnetic susceptibility χ_0 is estimated based on the Langevin susceptibility model [26].

$$\chi_0 = \chi_i \frac{3}{\xi}\left(\coth\xi - \frac{1}{\xi}\right) \quad (10)$$

$$\xi = \frac{\mu_0 M_d H V_M}{k_b T} \quad (11)$$

Moreover, the initial magnetic susceptibility is determined using the following relation [27]:

$$\chi_i = \frac{\mu_0 \varphi {M_d}^2 V_M}{3k_b T} \quad (12)$$

The degree of tissue injury due to the hyperthermia process can be evaluated by the Arrhenius kinetic model as follows [20]:

$$\frac{\partial \alpha}{\partial t} = (1-\alpha)^n A e^{-\frac{\Delta E}{RT}} \quad (13)$$

In this equation, α represents the degree of tissue injury, n denotes the polynomial order, R is the universal gas constant (8.314 $JK^{-1}mol^{-1}$), and T is the tissue temperature. Parameters A and ΔE are frequency factor and activation energy and are dependent on the type of tissue and have been characterized for different tissue types. Moreover, the properties of all materials used in the present study are summarized in Table 1.

Table 1: Properties of all materials used in the present study [20, 28-30]

Materials	$\rho(\frac{kg}{m^3})$	$C_p(\frac{J}{kg.k})$	$K(\frac{W}{m.k})$	$Q_{met}(\frac{W}{m^3})$	$w_b(\frac{1}{s})$
FCG tissue	1050	3770	0.48	700	0.0067
Tumor	1050	3852	0.54	5790	0.005
Blood	1050	3617	0.52	-	-
MNPs	5180	670	9.7	-	-
Liver	1079	3540	0.52	-	-

2-3- Solution method and boundary conditions

Heat transfer within the liver tissue, including the tumor region embedded with magnetic nanoparticles, was transiently modeled using the Pennes bioheat equation. The computational domain consisted of a three-dimensional geometric model replicating the actual liver anatomy, where the tumor region was defined as a separate subdomain incorporating a volumetric heat source due to the nanoparticles. The governing equation was solved numerically using the finite element method over a specified time interval. Physical properties of healthy liver tissue and tumor were assigned based on values reported in the literature. A constant temperature boundary condition of 37°C was applied on the entire external surface of the liver to simulate thermal equilibrium with the surrounding biological

environment. Convective heat transfer at the boundaries was neglected, as the model represents an isolated portion of the liver. The volumetric heat generation caused by the nanoparticles within the tumor was included as an internal heat source term in the Pennes bioheat equation. The transient solution was obtained using a direct solver with an appropriately chosen time step. To enhance accuracy within the tumor region, a finer and more refined mesh was employed.

3- Results and discussion

To validate the complex liver model, a simplified one-dimensional spherical radial model was utilized. Owing to its simpler geometric symmetry and faster numerical solvability, the spherical model provided a reliable basis for comparing and verifying the accuracy of heat transfer results under similar conditions. Although the liver geometry is inherently complex and non-spherical, the spherical model results serve as a credible benchmark for validating the key aspects of heat transfer and assessing the impact of magnetic nanoparticles in thermal therapy.

For validation purposes, the numerical results were compared against the study conducted by Lin and Liu [31]. In this validation scenario, the volumetric heat generation of the nanoparticles was fixed at $P=3.97\times10^5$ W/m3 as reported in the referenced paper. As illustrated in Fig. 4, the current results demonstrate excellent agreement with the previous study. The calculated error was less than 1%, confirming the accuracy and reliability of the model.

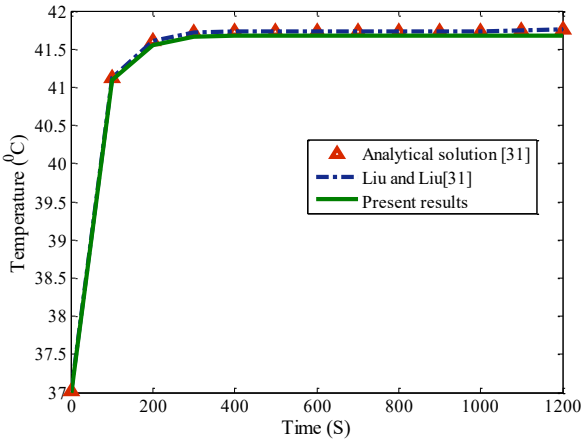

Fig. 4 Comparison and validation of the current results with the data reported by Lin and Liu [31]

3-1- Effect of magnetic field strength

Figure 5 illustrates the temporal evolution of temperature in magnetic nanoparticles subjected to three different magnetic field intensities (H=10, 14, and 18 kA/m). The results clearly demonstrate that both the temperature rise and the heating rate increase significantly with higher magnetic field strengths. At the initial stages, the temperature curves for all three field intensities remain nearly identical, indicating a similar thermal response delay in the system. However, as time progresses, the curves diverge, and the differences in their slopes become increasingly evident. The steepest temperature increase is observed for the field intensity of H=18 kA/m, highlighting the pronounced effect of strong magnetic fields in activating nanoparticles and enhancing heat generation via hysteresis losses and nanoparticle oscillations in the alternating field. In contrast, the field strength of H=10 kA/m results in a more gradual temperature rise, suggesting lower efficiency in magnetic energy absorption and conversion into thermal energy. These findings underscore the critical importance of optimizing magnetic field intensity for clinical hyperthermia applications, particularly in scenarios where rapid

attainment of therapeutic temperatures is essential for the selective ablation of tumor cells.

Figure 6 presents the temporal evolution of induced tissue damage under varying magnetic field intensities. The results clearly indicate that the extent of damage increases over time, with magnetic field strength playing a pivotal role in modulating this progression. In the early stages, damage levels are nearly identical across all field intensities, reflecting a uniform initial system response. However, as time advances, the curves begin to diverge, with stronger magnetic fields producing a steeper and more rapid increase in damage. This trend highlights the greater efficiency of higher field strengths in inducing thermal and mechanical effects within the target medium. The growing separation between the damage profiles over time underscores the decisive impact of field intensity on the rate and magnitude of tissue disruption. These findings emphasize the critical need for precise control over magnetic field strength in the development of optimized magnetic hyperthermia protocols, ensuring maximal therapeutic benefit while minimizing unintended side effects.

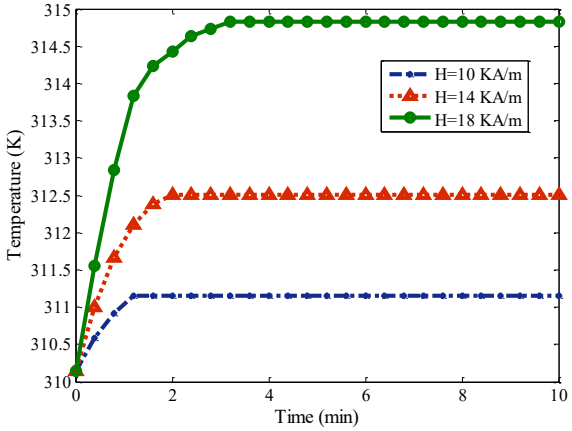

Fig. 5 Temporal Temperature Variation under Different Alternating Magnetic Field Strengths *(Platinum Ferrite Nanoparticles, D=6 nm, f=300 kHz)*

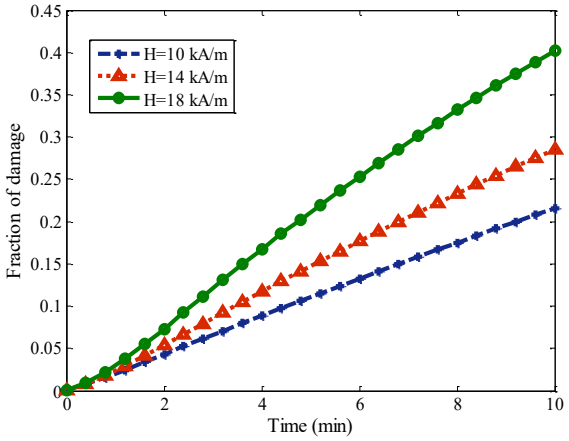

Fig. 6 Effect of Alternating Magnetic Field Strength on Tissue Damage *(Platinum Ferrite Nanoparticles, D=6 nm, f=300 kHz)*

3-2- Effect of magnetic field frequency

Figure 7 clearly demonstrates that increasing the frequency of the applied magnetic field leads to a more rapid rise in the temperature of magnetic nanoparticle-containing samples. In this process, frequency plays a pivotal role in determining the amount of energy transferred from the field to the nanoparticles. Higher frequencies result in more intense magnetic oscillations, which in turn enhance the rotational and translational motion of nanoparticles within the medium. This dynamic behavior intensifies energy dissipation through mechanisms such as hysteresis losses, Néel relaxation, and Brownian motion, ultimately leading to elevated heat generation. Although temperature increases are observed at lower frequencies, the rate of this increase is significantly slower, indicating limited field–nanoparticle interactions. As frequency rises, the heating curves become steeper, reflecting a higher rate of thermal energy production. These findings underscore the critical importance of frequency optimization in the design of magnetic nanoparticle-mediated hyperthermia therapies. An appropriately selected frequency can

facilitate faster and more efficient achievement of therapeutic temperatures, which is essential for precise planning of non-invasive cancer treatments.

Figure 8 illustrates that increasing the frequency of the magnetic field accelerates the rate of damage within the studied system. Notably, at a frequency of 700 kHz, the extent of damage increases with a steeper slope compared to lower frequencies. This behavior indicates that higher frequencies not only enhance the thermal power of the field but also significantly affect the intensity and rate of energy interaction with the magnetic nanoparticles. In magnetic nanoparticle-based therapeutic systems, frequency serves as a key parameter in determining the efficacy of hyperthermia treatments. Elevated frequencies lead to more efficient nanoparticle excitation and greater energy dissipation in the form of heat, which can induce localized damage to targeted cells, particularly tumor cells. At lower frequencies, damage still progresses but more slowly, underscoring the importance of precise frequency control in biomedical applications like targeted tumor ablation to maximize tumor damage while minimizing harm to healthy tissue.

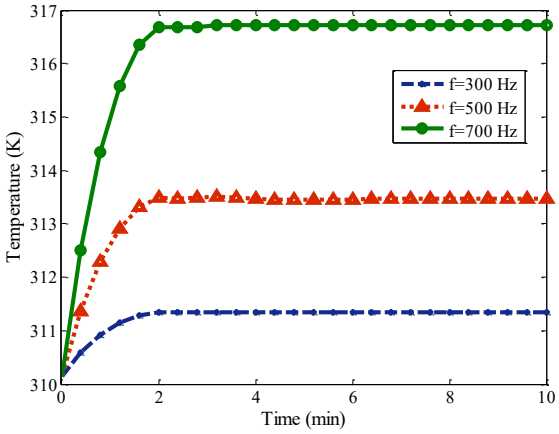

Fig. 7 Temporal temperature variation as a function of alternating magnetic field frequency *(platinum ferrite nanoparticles, D=6 nm, H=10 kA/m)*

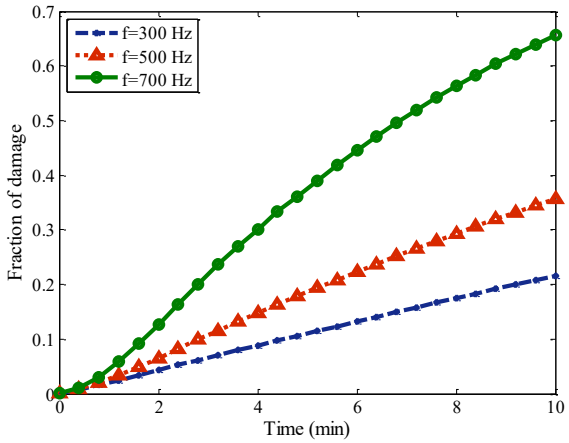

Fig. 8 Effect of Alternating Magnetic Field Frequency on Tissue Damage *(Platinum Ferrite Nanoparticles, D=6 nm, H=10 kA/m)*

3-3- Effect of nanoparticle diameter

Figure 9 illustrates the influence of magnetic nanoparticle diameter on the rate of temperature increase over time. The plotted curves reveal that larger nanoparticle diameters result in a faster temperature rise. Specifically, nanoparticles with a diameter of 7 nm exhibit a steeper temperature increase and reach higher temperatures in a shorter time compared to smaller particles with a diameter of 5 nm. In all cases, temperature rises with time; however, the variation in heating rates highlights the critical role of particle size in thermal performance. This difference can be attributed to the greater energy absorption capacity of larger nanoparticles under an alternating magnetic field. A larger diameter is typically associated with a higher magnetic volume, which enhances energy losses through mechanisms such as hysteresis and Néel or Brownian relaxations—ultimately resulting in greater heat generation. In contrast, smaller nanoparticles, especially those within the superparamagnetic range, tend to exhibit reduced heating efficiency due to their limited ability to retain remanent magnetization. These findings emphasize the importance of selecting an

optimal nanoparticle size to maximize hyperthermia efficacy and to achieve precise thermal control within the targeted treatment region.

Figure 10 illustrates the progression of tissue damage over time for different nanoparticle diameters, all exhibiting an increasing trend. However, nanoparticles with a larger diameter (D=7 nm) induce more substantial damage within the same time interval compared to smaller ones. This indicates that larger nanoparticles cause damage at a faster rate and reach higher levels of thermal injury more rapidly. This behavior can be explained by the greater ability of larger nanoparticles to absorb and transfer energy. As the particle diameter increases, so do the magnetic volume and the capacity to absorb energy from the alternating magnetic field, leading to enhanced heat generation and accelerated localized tissue damage. Consequently, larger nanoparticles can deliver more potent therapeutic effects in a shorter period. These findings highlight the critical role of nanoparticle size in optimizing magnetic hyperthermia treatments. Selecting an appropriate particle diameter can enhance therapeutic efficacy while minimizing off-target effects and preserving healthy tissue.

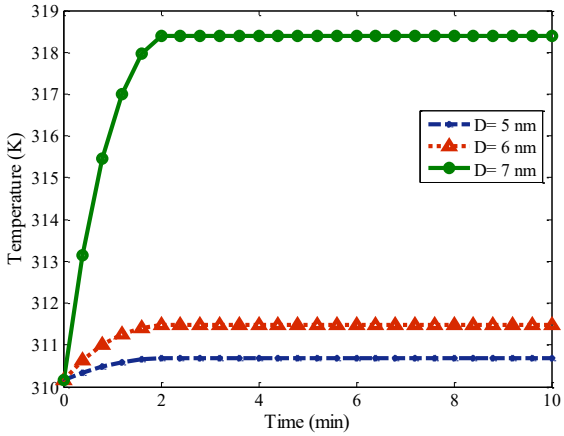

Fig. 9 temporal temperature changes as a function of nanoparticle size *(f=300 kHz, H=10 kA/m, platinum ferrite nanoparticles)*

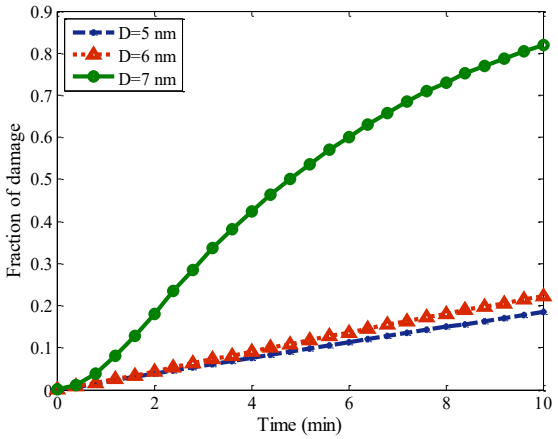

Fig. 10 effect of nanoparticle diameter on tissue damage over time *(platinum ferrite nanoparticles, D=6 nm, f=300 kHz)*

3-4- Effect of nanoparticle type

Figure 11 clearly demonstrates the hyperthermia performance of different nanoparticles under an external magnetic field. Among the evaluated materials, platinum ferrite ($PtFe_2O_4$) nanoparticles exhibit a notably faster and more pronounced temperature rise due to their more efficient magnetic energy absorption. This nanoparticle reaches a stable therapeutic temperature in a significantly shorter time compared to the others, indicating its superior capability in converting magnetic energy into heat. In contrast, cobalt ferrite ($CoFe_2O_4$) and iron(III) oxide (Fe_2O_3) nanoparticles show a slower temperature increase, likely attributed to inherent differences in their magnetic properties, crystal structures, and energy absorption capacities. These variations influence the extent of hysteresis losses and other heat generation mechanisms, ultimately affecting the overall hyperthermia performance. Therefore, selecting nanoparticles with favorable magnetic characteristics plays a pivotal role in enhancing the efficiency of magnetic hyperthermia treatments.

Figure 12 depicts the temporal variation in tissue necrosis induced by different types

of nanoparticles. As observed, platinum ferrite ($PtFe_2O_4$) nanoparticles exhibit the highest rate and extent of necrosis, indicating their superior capability in inducing thermal damage to tissue. Cobalt ferrite ($CoFe_2O_4$) nanoparticles rank second, with a slower necrosis progression compared to platinum ferrite. Iron(III) oxide (Fe_2O_3) nanoparticles show the lowest necrosis levels and the slowest rate of tissue damage. These discrepancies in nanoparticle performance can be attributed to differences in their structural and magnetic properties, which directly affect heat generation efficiency and subsequent tissue injury.

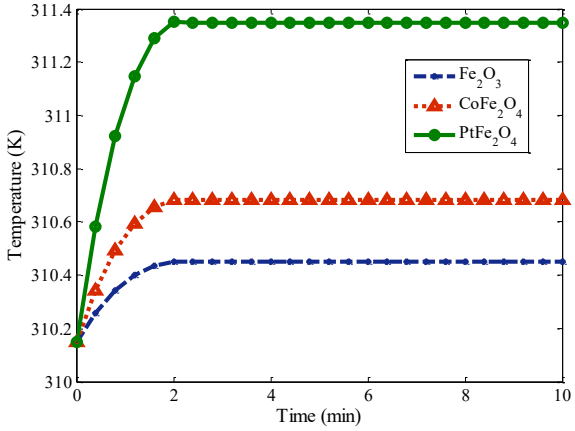

Fig. 11 temporal temperature evolution for various magnetic nanoparticles *(D=6 nm, f=300 kHz, H=10 kA/m)*

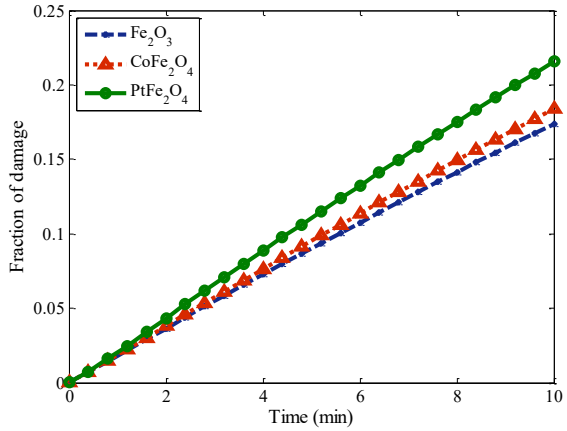

Fig. 12 Time-dependent tissue destruction induced by various magnetic nanoparticles *(D=6 nm, f=300 kHz, H=10 kA/m)*

Table 2 presents a quantitative comparison of the effects of key parameters on local temperature rise and tissue damage during magnetic nanoparticle hyperthermia. The analysis indicates that nanoparticle diameter exerts the most significant influence on both temperature elevation and thermal injury. Increasing the particle size from 5 to 7 nm raised the peak temperature from 310.5 to 318.4 K ($\Delta T \approx +7.9$ K) and the tissue damage fraction from 19% to 82%.

The magnetic field frequency also exhibited a considerable effect ($\Delta T \approx +5.5$ K and $\Delta Damage \approx +44\%$), though less pronounced than that of particle size. Variation in field intensity (10→18 kA/m) resulted in a moderate temperature rise of approximately 3.7 K and an increase in tissue damage by 18%. Among the evaluated materials, the nanoparticle type (Fe_2O_3, $CoFe_2O_4$, $PtFe_2O_4$) had the least influence, producing less than 1 K temperature variation; however, $PtFe_2O_4$ exhibited the highest heating efficiency.

These results highlight the nonlinear relationship between temperature and tissue damage, as described by the Arrhenius model, where even small temperature increments can result in a substantial increase in thermal injury. This nonlinear behavior arises because the rate of cellular protein denaturation and membrane disruption increases exponentially with temperature.

Consequently, once the threshold temperature for irreversible damage (typically around 316–318 K) is exceeded, tissue viability decreases rapidly, leading to localized necrosis. Therefore, precise thermal control is essential in magnetic nanoparticle hyperthermia to maximize tumor ablation while preventing collateral injury to surrounding healthy tissues.

Table 2: Quantitative Comparison and Analysis of Simulation Results

Parameter	Value / Type	Maximum Temperature (K)	Tissue Damage after 600s (%)
Magnetic field intensity (kA/m)	10 → 18	311.2 → 314.9	23 → 41
Magnetic field frequency (kHz)	300 → 700	311.3 → 316.8	22 → 66
Nanoparticle diameter (nm)	5 → 7	310.5 → 318.4	19 → 82
Nanoparticle type	Fe_2O_3 / $CoFe_2O_4$ / $PtFe_2O_4$	310.44 / 310.7 / 311.37	17 / 18 / 22

4-Conclusion

This study presents, for the first time, a comprehensive investigation into the effects of key parameters—including magnetic field intensity and frequency, as well as the size and type of magnetic nanoparticles—on magnetic hyperthermia treatment within realistic liver tissue. The results demonstrated that increasing the intensity and frequency of the magnetic field enhances both the heating rate and targeted thermal damage. Moreover, nanoparticles with larger diameters and optimized magnetic properties, such as $PtFe_2O_4$, exhibited superior heat generation and selective cellular damage compared to other samples. These findings highlight the critical role of the physical and magnetic characteristics of nanoparticles in regulating therapeutic temperature and treatment efficacy. Although a quantitative optimization framework was not implemented in this study, the results provide valuable insights into the trends and interactions of key parameters, serving as a foundation for future optimization studies. Importantly, the outcomes underscore the potential to rationally design safer and more effective nanoparticle-based hyperthermia protocols, particularly for temperature-sensitive liver tissue. Overall, this work represents a significant step toward the development of non-invasive, safe, and effective magnetic hyperthermia therapies for liver cancer, while also identifying the need for future quantitative optimization to refine treatment protocols.

5- Limitations and Future Work

The present model has several important limitations that should be acknowledged:

- Simplified liver physiology: Convective effects and variability of blood perfusion were not incorporated.
- Limited validation: The model was validated against a single prior numerical study, and multiple experimental datasets for comprehensive validation are unavailable.
- Lack of quantitative optimization framework: Parameter analysis was analytical, and a full optimization framework to determine precise and safe treatment conditions was not developed.
- Generic, non-patient-specific modeling: The current model is based on generic anatomy and does not incorporate patient-specific geometries for clinical application.

Future studies could address these limitations and further improve the biological accuracy of the model, including:

- Incorporating dynamic blood perfusion and convective heat transfer within the hepatic vascular network.
- Developing a quantitative optimization framework to determine precise, safe, and effective hyperthermia conditions.

- Implementing patient-specific modeling based on realistic anatomical geometries to enhance clinical applicability and enable personalized treatment strategies.

These advancements would represent a significant step toward increasing the accuracy, reliability, and effectiveness of magnetic nanoparticle-based hyperthermia for liver cancer therapy.

Acknowledgment

The authors sincerely acknowledge Islamic Azad University, Ramsar Branch, for providing the financial support that made this study possible.

References

[1] Cavaliere, R., Ciocatto, E. C., Giovanella, B. C., Heidelberger, C., Johnson, R. O., Margottini, M., ... & Rossi-Fanelli, A. (1967). Selective heat sensitivity of cancer cells. Biochemical and clinical studies. *Cancer*, *20*(9), 1351-1381.

[2] Robinson, J. E., Wizenberg, M. J., & McCready, W. A. (1974). Combined hyperthermia and radiation suggest an alternative to heavy particle therapy for reduced oxygen enhancement ratios. *Nature*, *251*(5475), 521-522.

[3] Steeves, R. A. (1992). Hyperthermia in cancer therapy: where are we today and where are we going?. *Bulletin of the New York Academy of Medicine*, *68*(2), 341.

[4] Dewey, W. C. (1994). Arrhenius relationships from the molecule and cell to the clinic. *International journal of hyperthermia*, *10*(4), 457-483.

[5] Siperstein, A. E., Rogers, S. J., Hansen, P. D., & Gitomirsky, A. (1997). Laparoscopic thermal ablation of hepatic neuroendocrine tumor metastases. *Surgery*, *122*(6), 1147-1155.

[6] Goldberg, S. N., Gazelle, G. S., Solbiati, L., Livraghi, T., Tanabe, K. K., Hahn, P. F., & Mueller, P. R. (1998). Ablation of liver tumors using percutaneous RF therapy. *AJR. American journal of roentgenology*, *170*(4), 1023-1028.

[7] Lencioni, R., Goletti, O., Armillotta, N., Paolicchi, A., Moretti, M., Cioni, D., ... & Bartolozzi, C. (1998). Radio-frequency thermal ablation of liver metastases with a cooled-tip electrode needle: results of a pilot clinical trial. *European radiology*, *8*(7), 1205-1211.

[8] Nagata, Y., Hiraoka, M., Nishimura, Y., Masunaga, S., Mitumori, M., Okuno, Y., ... & Fukuda, Y. (1997). Clinical results of radiofrequency hyperthermia for malignant liver tumors. *International Journal of Radiation Oncology* Biology* Physics*, *38*(2), 359-365.

[9] Petryk, A. A., Giustini, A. J., Gottesman, R. E., Trembly, B. S., & Hoopes, P. J. (2013). Comparison of magnetic nanoparticle and microwave hyperthermia cancer treatment methodology and treatment effect in a rodent breast cancer model. *International Journal of Hyperthermia*, *29*(8), 819-827.

[10] Coughlin, C. T. (2023). Prospects for interstitial hyperthermia. In *Interstitial hyperthermia: physics, biology and clinical aspects* (pp. 1-10). CRC Press.

[11] Radmilović-Radjenović, M., Bošković, N., & Radjenović, B. (2022). Computational modeling of microwave tumor ablation. *Bioengineering*, *9*(11), 656.

[12] Yang, X., Liao, Y., Fan, L., Lin, B., Li, J., Wu, D., ... & Du, X. (2024). High-intensity focused ultrasound ablation combined with immunotherapy for treating liver metastases: A prospective non-randomized trial. *Plos one*, *19*(7), e0306595.

[13] Tam, A., Contreras, K., Fall, F., Maxwell, A., Liu, J. B., Forsberg, F., ... & Koenig, G. (2025). Development of a contrast-enhanced ultrasound–guided high-intensity focused ultrasound system for coagulation of liver parenchyma. *Journal of Trauma and Acute Care Surgery*, *98*(4), 662-666.

[14] Seaton, M. P., Schmidt, J. C., Brown, N. J., Sahyouni, R., Khalessi, A. A., Ben-Haim, S., & Gonda, D. D. (2025). Contemporary applications of laser interstitial thermal therapy: A comprehensive systematic review. *World Neurosurgery*, *193*, 356-372.

[15] Zhao, X., Li, R., Guo, Y., Wan, H., & Zhou, D. (2024). Laser interstitial thermal therapy for recurrent glioblastomas: a systematic review and meta-analysis. *Neurosurgical Review*, *47*(1), 159.

[16] Fakhradini, S. S., Mosharaf-Dehkordi, M., & Ahmadikia, H. (2025). A numerical study on

optimization of microwave antenna power for liver cancer therapy enhanced with hybrid magnetic nanoparticles. *Journal of Thermal Biology*, 104117.

[17] Zhang, L., Li, Q., Liu, J., Deng, Z., Zhang, X., Wang, K., ... & Sun, K. (2025). Precise size control of superparamagnetic Fe3O4 nanoparticles for liver cancer diagnosis and magnetic hyperthermia therapy. *Colloids and Surfaces B: Biointerfaces*, 114763.

[18] Minbashi, M., Kordbacheh, A. A., Ghobadi, A., & Tuchin, V. V. (2020). Optimization of power used in liver cancer microwave therapy by injection of Magnetic Nanoparticles (MNPs). *Computers in biology and medicine*, *120*, 103741.

[19] Andreozzi, A., Brunese, L., Cafarchio, A., Netti, P., & Vanoli, G. P. (2025). Effects of magnetic nanoparticle distribution in cancer therapy through hyperthermia. *International Journal of Thermal Sciences*, *208*, 109428.

[20] Rahpeima, R., & Lin, C. A. (2022). Numerical study of magnetic hyperthermia ablation of breast tumor on an anatomically realistic breast phantom. *Plos one*, *17*(9), e0274801.

[21] Mahesh, N., Singh, N., & Talukdar, P. (2023). A mathematical model of intratumoral infusion, particle distribution and heat transfer in cancer tumors: In-silico investigation of magnetic nanoparticle hyperthermia. *International Journal of Thermal Sciences*, *183*, 107887.

[22] Gas, P., Miaskowski, A., & Subramanian, M. (2020). In silico study on tumor-size-dependent thermal profiles inside an anthropomorphic female breast phantom subjected to multi-dipole antenna array. *International Journal of Molecular Sciences*, *21*(22), 8597.

[23] Suleman, M., & Riaz, S. (2020). 3D in silico study of magnetic fluid hyperthermia of breast tumor using Fe3O4 magnetic nanoparticles. *Journal of thermal biology*, *91*, 102635.

[24] Pennes, H. H. (1948). Analysis of tissue and arterial blood temperatures in the resting human forearm. *Journal of applied physiology*, *1*(2), 93-122.

[25] Maenosono, S., & Saita, S. (2006). Theoretical assessment of FePt nanoparticles as heating elements for magnetic hyperthermia. *IEEE transactions on magnetics*, *42*(6), 1638-1642.

[26] Rosensweig, R. E. (2002). Heating magnetic fluid with alternating magnetic field. *Journal of magnetism and magnetic materials*, *252*, 370-374.

[27] Belc, D., Haik, Y., Chen, C. J., Roberts, R., & Arora, R. (2004, December). Effect of high AC magnetic field on magnetic nanoparticles for magnetic hyperthermia and radiation/chemotherapy applications. In *IEEE International Workshop on Biomedical Circuits and Systems, 2004.* (pp. S1-4). IEEE.

[28] Soltani, M., Rahpeima, R., & Kashkooli, F. M. (2019). Breast cancer diagnosis with a microwave thermoacoustic imaging technique—a numerical approach. *Medical & biological engineering & computing*, *57*(7), 1497-1513.

[29] Rahpeima, R., Soltani, M., & Kashkooli, F. M. (2020). Numerical study of microwave induced thermoacoustic imaging for initial detection of cancer of breast on anatomically realistic breast phantom. *Computer Methods and Programs in Biomedicine*, *196*, 105606.

[30] Bagheli, S., Fadafan, H. K., Orimi, R. L., & Ghaemi, M. (2015). Synthesis and experimental investigation of the electrical conductivity of water based magnetite nanofluids. *Powder Technology*, *274*, 426-430.

[31] Lin, C. T., & Liu, K. C. (2009). Estimation for the heating effect of magnetic nanoparticles in perfused tissues. *International Communications in Heat and Mass Transfer*, *36*(3), 241-244.